Conserved Glu-47 and Lys-50 residues are critical for UDP-*N*-acetylglucosamine/UMP antiport activity of the mouse Golgi-associated transporter Slc35a3

Received for publication, April 13, 2019, and in revised form, May 9, 2019 Published, Papers in Press, May 22, 2019, DOI 10.1074/jbc.RA119.008827

M. Agustina Toscanini[‡1,2], **M. Belén Favarolo**[‡1,3], **F. Luis Gonzalez Flecha**[‡4], **Berit Ebert**[§5], **Carsten Rautengarten**[§], and **Luis M. Bredeston**[‡4,6]

From the [‡]*Departamento de Química Biológica-IQUIFIB, Facultad de Farmacia y Bioquímica, Universidad de Buenos Aires-CONICET, Ciudad Autónoma de Buenos Aires, Junín 956 (1113), Argentina and the* [§]*School of BioSciences, University of Melbourne, Melbourne, Victoria 3010, Australia*

Edited by Gerald W. Hart

Nucleotide sugar transporters (NSTs) regulate the flux of activated sugars from the cytosol into the lumen of the Golgi apparatus where glycosyltransferases use them for the modification of proteins, lipids, and proteoglycans. It has been well-established that NSTs are antiporters that exchange nucleotide sugars with the respective nucleoside monophosphate. Nevertheless, information about the molecular basis of ligand recognition and transport is scarce. Here, using topology predictors, cysteine-scanning mutagenesis, expression of GFP-tagged protein variants, and phenotypic complementation of the yeast strain Kl3, we identified residues involved in the activity of a mouse UDP-GlcNAc transporter, murine solute carrier family 35 member A3 (mSlc35a3). We specifically focused on the putative transmembrane helix 2 (TMH2) and observed that cells expressing E47C or K50C mSlc35a3 variants had lower levels of GlcNAc-containing glycoconjugates than WT cells, indicating impaired UDP-GlcNAc transport activity of these two variants. A conservative substitution analysis revealed that single or double substitutions of Glu-47 and Lys-50 do not restore GlcNAc glycoconjugates. Analysis of mSlc35a3 and its genetic variants reconstituted into proteoliposomes disclosed the following: (i) all variants act as UDP-GlcNAc/UMP antiporters; (ii) conservative substitutions (E47D, E47Q, K50R, or K50H) impair UDP-GlcNAc uptake; and (iii) substitutions of Glu-47 and Lys-50 dramatically alter kinetic parameters, consistent with a critical role of these two residues in mSlc35a3 function. A bioinformatics analysis revealed that an E*XX*K motif in TMH2 is highly conserved across SLC35 A subfamily members, and a 3D-homology model predicted that Glu-47 and Lys-50 are facing the central cavity of the protein.

Nucleotide sugars play a key role as precursors for the biosynthesis of glycoconjugates in the secretory pathway. These activated sugar donors serve as substrates for glycosyltransferases. Although they are on the cytoplasmic side of the endoplasmic reticulum (ER),[7] they allow the attachment of sugars to dolichol phosphate to form glycosylated lipid precursors, and within the Golgi lumen, they are required for the glycosylation of proteins, lipids, and proteoglycans. To enable the latter and to overcome the subcellular partitioning of substrates and enzymes, nucleotide sugars are required to be imported from the cytoplasm into the Golgi lumen by specific membrane proteins, the so-called nucleotide sugar transporters (NSTs) (1, 2). The physiological relevance of this transport process is well-documented from unicellular (3) to multicellular organisms (4, 5), whereas mutations that impair NST function are associated with severe developmental phenotypes.

Based on biochemical (6) and genetic approaches (7), an antiport mechanism exchanging a nucleotide sugar with the corresponding nucleoside monophosphate has been proposed for NST function (2). The cloning, expression, and functional characterization of more than 60 NSTs from diverse species revealed that some of them act as monospecific transporters, whereas others turned out to have the capability of transporting multiple substrates in a competitive or simultaneous process (8–17).

Based on sequence analyses, mammalian NSTs were classified as members of the solute carrier 35 family (SLC35), together with 3′-phosphoadenosine–5′-phosphosulfate (18) and ATP transporters (19). However, of the 24 members of the SLC35 subfamilies A–G, only half have been experimentally characterized in different species, including humans (18). In

This work was supported by the National Research Council (CONICET, Argentina) Grant PIP-11220090100811, and University of Buenos Aires Travel Award (to L. M. B.). The authors declare that they have no conflicts of interest with the contents of this article.
This article contains Figs. S1–S5 and Tables S1 and S2.

[1] Both authors contributed equally to this work.

[2] Present address: Dept. de Biotecnología, Facultad de Farmacia y Bioquímica, Universidad de Buenos Aires, CABA, 1113 Argentina.
[3] Present address: Instituto de Biología Celular y Neurociencias "Prof. E. De Robertis," Facultad de Medicina, Universidad de Buenos Aires-CONICET, CABA, 1121 Argentina.
[4] Career Investigators of the National Research Council (CONICET, Argentina).

[5] Supported by Australian Research Council Future Fellowship FT160100276, Discovery Grant DP180102630 and Mizutani Foundation for Glycoscience Grant 18-0237.

[6] To whom correspondence should be addressed: Dept. de Química Biológica-IQUIFIB, Facultad de Farmacia y Bioquímica, Universidad de Buenos Aires-CONICET, Ciudad Autónoma de Buenos Aires, Junín 956 (1113), Argentina. Tel.: 5411-52874794; Fax: 5411-49625457; E-mail: bredes@qb.ffyb.uba.ar.

[7] The abbreviations used are: ER, endoplasmic reticulum; NST, nucleotide sugar transporter; TMH2, transmembrane helix 2; PDB, Protein Data Bank; 3-PGA, 3-phosphoglycerate; CL, cysteine-less; CMP-SA, CMP-sialic acid; DMT, drug/metabolite transporter.

humans, mutations of five NSTs of the SLC35 family with diverse substrate specificities, namely A1 (20, 21), A2 (22, 23), A3 (24), C1 (25–27), and D1 (28), are linked to congenital disorders of glycosylation that cause diverse severe neurological and skeletal anomalies.

Among the Slc35 family, subfamily A is the most thoroughly characterized. For three of its five members substrate specificities have been identified. A1, A2, and A3 are specific for CMP-sialic acid (CMP-SA) (29), UDP-galactose (UDP-Gal) (30), and UDP-GlcNAc (31), respectively. Studies determining the topology of the mouse CMP-SA transporter Slc35a1, using a epitope-insertion technique, indicated a 10-transmembrane protein with the N and C termini facing the cytosol (32). Furthermore, studies using chimeric mutants of A1 and A2 (33, 34), as well as mutational analyses (35, 36), identified transmembrane domains and residues critically important for the recognition of CMP-SA as a substrate.

Another well-characterized member of the subfamily A, Slc35a3, is a Golgi-resident UDP-GlcNAc transporter present in multicellular organisms with high-sequence conservation from worms (4) to mammals (31). A mutation (V180F) in the predicted transmembrane helix 6 of Slc35a3 causes complex vertebral malformation in cattle (37), a lethal autosomal-recessive defect. Recently, mutations of the human SLC35A3 ortholog have been associated with autism spectrum disorder, epilepsy, and skeletal malformations. Affected patients carry variants containing single amino acid changes or truncated proteins (24, 38–40). Gene silencing of SLC35A3 in mammalian cell lines affects the biosynthesis of highly branched *N*-glycans and keratan sulfate (41) Furthermore, it has been reported that the UDP-Gal (Slc35a2) and UDP-GlcNAc (Slc35a3) transporters can associate with acetylglucosaminyltransferases (42) to form complexes, an observation that may be related to the sequential addition of the sugars GlcNAc, galactose, and sialic acid during the processing of glycoproteins.

Since the first observation of nucleotide sugar uptake into mouse liver microsomes (43), substantial efforts have been made to understand NST function and physiological relevance (1). However, information about the relationship between structure and function is still scarce, and mechanisms underpinning nucleotide sugar transport at the molecular level remain largely unknown. Recently, the first crystal structure of NST was determined. The obtained 3D model of the yeast Vrg4 GDP-mannose transporter provided crucial information to start understanding the molecular mechanisms of nucleotide sugar import into the Golgi (44).

Here, we report a simple approach to test the *in vivo* function of NSTs. This approach combined bioinformatic analyses, cysteine-scanning mutagenesis, GFP-based detection of protein expression, and phenotypic complementation of yeast mutants that allowed us to identify amino acids residues required for UDP-GlcNAc transport activity of the mouse Slc35a3. A detailed investigation of the transmembrane helix 2 from Slc35a3 identified two critical residues, glutamic acid 47 and lysine 50. Conservative replacements combined with *in vivo* and *in vitro* activity assays confirmed the significance of both residues for transport activity.

Results

Expression and transport activity of the mouse SLC35A3 assessed in yeast using a whole-cell fluorescence approach

Mouse Slc35a3 (mSLC35A3), a protein consisting of 326 amino acids, shares between 95 and 96% sequence identity with four mammalian SLC35A3 variants, which previously have been experimentally characterized as Golgi-localized UDP-GlcNAc transporters (31, 37, 45, 46). To confirm the substrate specificity of mSlc35a3, Kl3 cells, a mutant strain of the yeast *Kluveromyces lactis* lacking a functional UDP-GlcNAc transporter, were transformed with either the empty vector (plasmid pE4) or pE4mSLC35A3. Subsequently, the cells were incubated with GSII lectin conjugated to FITC (GSII–FITC), which specifically binds GlcNAc-containing glycoconjugates. Only the suspension of Kl3 cells transformed with pE4mSLC35A3 showed fluorescence levels similar to that of WT Kl8 cells, carrying the functional UDP-GlcNAc transporter, indicating that they recovered the ability to bind the lectin GSII–FITC (Fig. 1*A*, *dark gray bars*). In this *in vivo* system, UDP-GlcNAc transport activity, mediated by mSLC35A3, is indirectly evaluated through the restoration of GlcNAc-containing glycoconjugates at the surface of Kl3 cells. This implicates at least three steps as follows: the restoration of the import of UDP-GlcNAc into the lumen of the Golgi apparatus through expression of an active transporter; the synthesis of GlcNAc glycoconjugates by specific lumenal transferases; and an appropriate membrane cell-sorting process of these products (47).

One aim of this work was to generate a collection of mutants and conveniently test their expression while avoiding time-consuming methods. To achieve this, the sequence of the green fluorescent protein (GFP) was fused to mSlc35a3. As shown in Fig. 1*C*, perinuclear fluorescence in Kl3 cells transformed with mSLC35A3–GFP can be visualized by confocal microscopy, consistent with the expression of mSlc35a3–GFP in the secretory pathway. Subsequent spectrofluorimetric measurements of the cell suspensions showed an increase in GFP fluorescence compared with cells transformed with the empty vector (pE4) or pE4m*slc35a3* (Fig. 1*A*, *white bars*). Heating the cell suspensions for 1 min at 90 °C reduced the fluorescence signal of mSlc35a3–GFP-expressing cells to background levels of the control cells transformed with the empty vector. This is most likely due to the irreversible denaturation of the GFP fusion protein (Fig. 1, *A*, *gray bars*, and *C*).

The results presented in Fig. 1*A* indicate that fusing GFP to mSlc35a3 did not significantly alter its transport capacity (Fig. 1*B*) as revealed by the binding of the lectin. Next, the V180F mutation that had been shown to impair transport activity of the bovine Slc35a3 transporter (37) was introduced into the mouse SLC35A3 sequence, and subsequently the Slc35a3 mutant was expressed as GFP fusion in K13 cells. Although the expression level of the mutated variant was higher than the WT protein (Fig. 1*A*, *white bars*), cells expressing the V180F variant bound less than 25% of the GSII–FITC lectin compared with cells expressing mSlc35a3–GFP (Fig. 1*B*). This indicates a substantial decrease in UDP-GlcNAc transport activity. Taken together, our results suggest that this approach, based on heterologous expression of GFP-tagged proteins combined with GSII–FITC lectin recognition of GlcNAc glycoconjugates, can

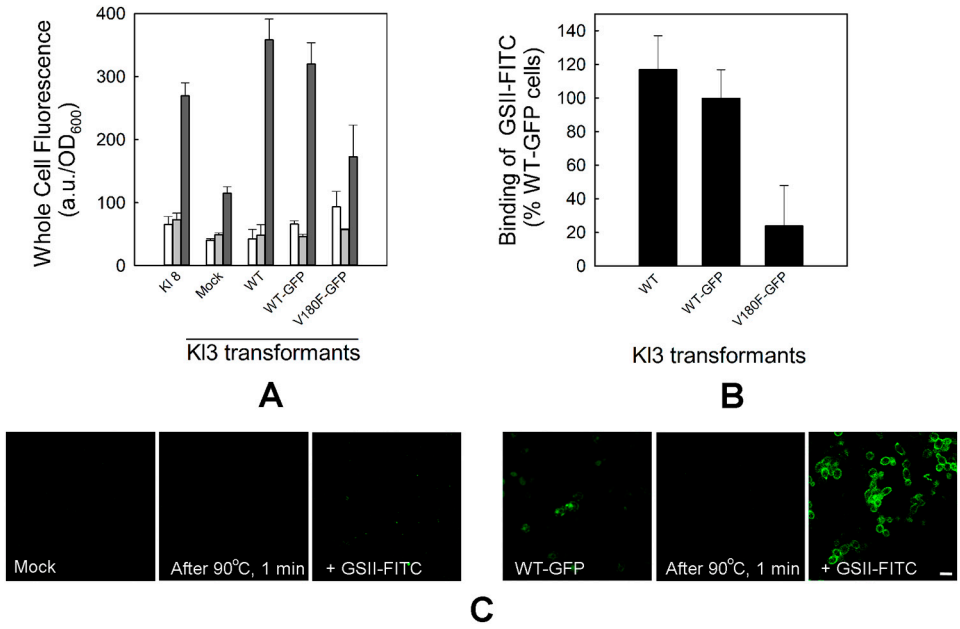

Figure 1. Expression of mSLC35A3 and phenotypic complementation of Kl3 cells. Kl8 cells were grown in YPD media, and Kl3 cells transformed with plasmid pE4 (*Mock*), pE4-mSLC35A3 (*WT*), pE4-mSLC35A3–GFP (*WT–GFP*), or pE4-V180F-GFP (*V180F-GFP*) were grown in −Ura media to an OD = 2.0. *A,* GFP fluorescence of the cell suspension was measured before (*white bars*) and after incubation at 90 °C for 1 min (*light gray bars*). The heated cells were incubated with GSII–FITC lectin, and fluorescence associated with cell suspensions was measured (*dark gray bars*). Fluorescence measurements were normalized to OD_{600} of the suspension and expressed as fluorescence arbitrary units (*a.u.*)/OD_{600}. *B,* fluorescence of GSII–FITC bound to Kl3 cells expressing mSLC35A3 and variants. Background fluorescence of mock cells was subtracted, and values are expressed as a percentage of WT–GFP. *Error bars* represent the mean and S.E. of three independent replicates. *C,* confocal microscopy fluorescence of Kl3 cells transformed with pE4 (*Mock*) or pE4-mSLC35A3GFP (*WT-GFP*) plasmids. *Scale bar,* 4 μm.

successfully be employed to evaluate the expression and activity of mSLC35A3.

Topology analysis of mSlc35a3

To identify amino acid residues relevant for transport activity, we first analyzed the primary amino acid sequence of mSlc35a3, using the topology predictors TOPCONS, MEMSAT-SVM, HMMTOP, and TMHMM. As summarized in Table S1, 8–10 transmembrane helices (TMHs) were predicted for mSLC35A3. The data obtained from the different prediction programs varied the most on TMHs 3 and 4, whereas TMHs 1–2 and 5–10 were predicted by all methods used, with slight extension differences (Fig. S1). Similar results were obtained for other well-characterized UDP-GlcNAc transporters from different species, including *Homo sapiens* and *Caenorhabditis elegans* as well as for different members of subfamily A, *e.g.* mouse Slc35a1, the only NST for which the topology has been experimentally determined (32). Based on this information, a 10-transmembrane helical model was proposed as an initial working hypothesis for mSlc35a3 (Fig. 2). Given the even number of TMHs and the positive inside rule (48), we conclude that both the N and C termini would be oriented to the cytoplasmic side. A general analysis of the amino acid distribution in the model showed an accumulation of charged and polar residues in luminal and cytoplasmic loops, whereas within the transmembrane helices hydrophobic residues prevailed. A detailed assessment of the transmembrane helices in the model revealed that five TMHs (1, 3, 4, 6, and 9) were enriched in amino acids with polar characteristics, whereas only three charged residues were identified, namely Glu-47 and Lys-50 located in TMH2 and Lys-120 in TMH4 (Table 1).

Cys-scanning mutagenesis of transmembrane helix 2

As shown in Fig. 2, the mSlc35a3 amino acid sequence contains three cysteine residues: Cys-54 in TMH2, Cys-64 in the loop between TMH2 and TMH3, and Cys-184 in TMH6. To generate a collection of cysteine-unique mutants, we first produced a cysteine-less variant (CL). Therefore, mSlc35a3 variant containing substitutions corresponding to C54S/C64S/C184S was generated and fused to GFP. The expression level of CL-GFP in Kl3 cells was similar to that of WT–GFP (Fig. S2). After incubation with GSII–FITC, cells bound close to 80% of the lectin compared with cells expressing the WT protein (Fig. 3). As assessed by phenotypic complementation of Kl3 cells, all cysteine replacements were well-tolerated by the protein, indicating that they are not essential for transport activity and concluding that the CL mutant is functionally active *in vivo*.

Based on the bioinformatic results obtained for the mSlc35a3 sequence (Fig. 2 and Table 1), further experimental analysis focused on the putative TMH2. Notably, TMH2, which was predicted by all membrane topology programs used in this study, is highly hydrophobic and contains two charged amino acids embedded in the membrane. Charged and polar residues in transmembrane domains of transport proteins are usually involved in the binding of hydrophilic substrates, domain interactions, or conformational changes as part of the transport mechanism (49). Consequently, the corresponding codon of each amino acid between leucine 38 to lysine 60 was substituted by a cysteine codon using CL as a backbone, and a collection of

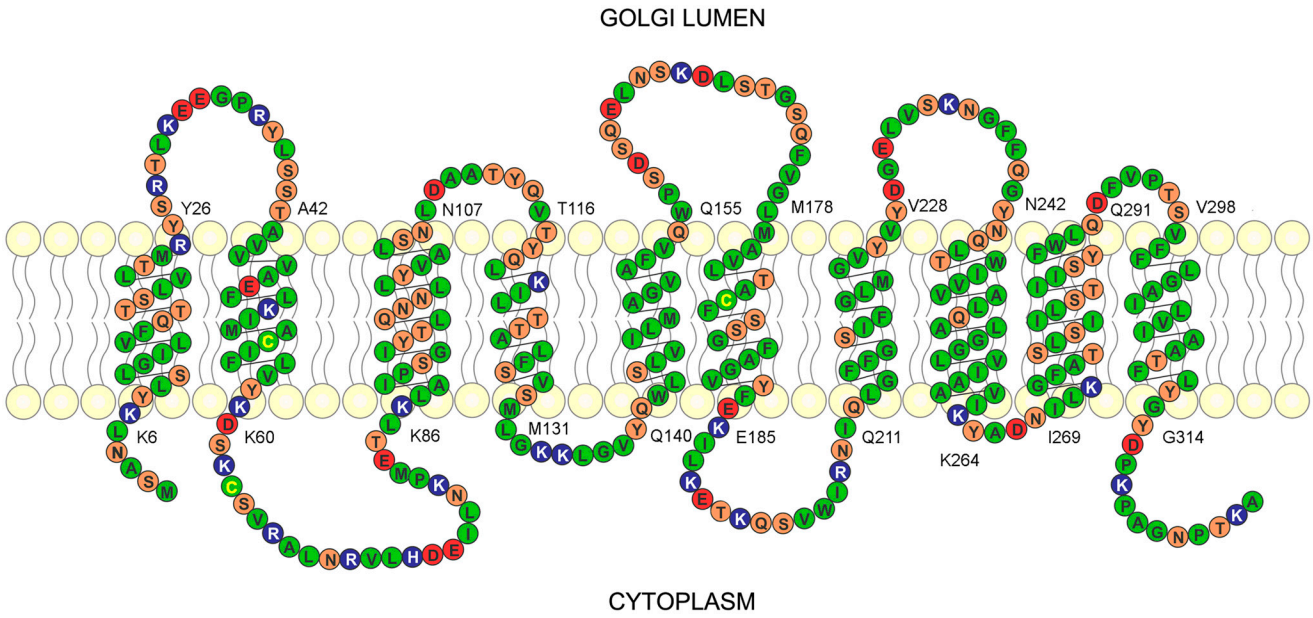

Figure 2. Ten transmembrane helices model of mSlc35a3. Amino acids with distinctive physicochemical properties are labeled as follows: *green* (nonpolar: Gly, Ala, Val, Cys, Pro, Leu, Ile, Met, Trp, and Phe), *orange* (polar: Ser, Thr, Tyr, Asn, and Gln), *blue* (positively charged: Lys, Arg, and His), and *red* (negatively charged: Asp and Glu). The three cysteines 54, 64, and 184 are highlighted in *yellow*.

Table 1

Polar and charged amino acid residues located within the predicted transmembrane helices of mSlc35a3. Charged residues are highlighted in bold

Transmembrane helices	Residue and no.
1	Ser-9, Gln-16, Thr-17, Thr-18, Ser-19, Thr-23
2	**Glu-47**, **Lys-50**
3	Ser-91, Tyr-94, Thr-95, Gln-97, Asn-98, Asn-99, Tyr-102
4	Gln-118, **Lys-120**, Thr-123, Thr-124, Ser-128
5	Ser-143
6	Thr-182, Ser-186, Ser-187
7	Ser-217
8	Thr-245, Gln-252
9	Thr-275, Ser-276, Ser-278, Ser-282, Thr-283, Ser-286, Tyr-287
10	Thr-310

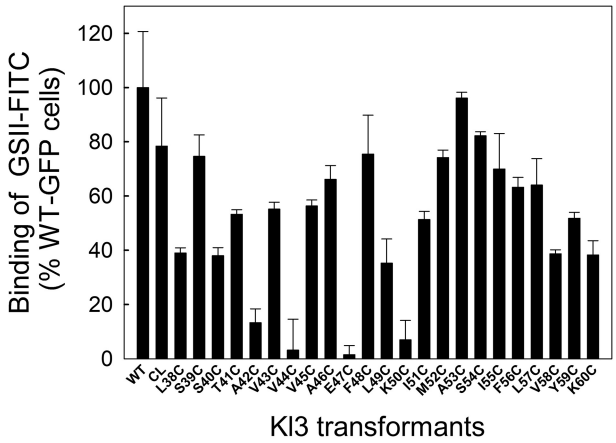

Figure 3. Analysis of cysteine-unique mutants by phenotypic complementation of KI3 cells. Cells were grown in −Ura media, heated, and incubated with GSII–FITC 1 h at room temperature. The fluorescence of GSII–FITC bound to KI3 cells was measured and expressed as percentage of the WT–GFP value. *Error bars* represent the mean and S.E. of three independent replicates.

23 cysteine-unique mutants fused to GFP was generated. As shown in Fig. S2, all KI3 transformants exhibited GFP fluorescence higher than cells transformed with the empty vector, which decreased to mock background levels after heat treatment. Incubation with GSII–FITC showed that most of the cells expressing cysteine-unique mutants bound the lectin, with fluorescence intensity values higher than 40% of the WT, consistent with a restoration of the UDP-GlcNAc import into the lumen of the Golgi apparatus (Fig. 3). The only exceptions were mutants A42C, V44C, E47C, and K50C, which revealed a specific binding of GSII–FITC lower than 20% that of WT cells, indicative of a severe impairment of transport activity.

Phenotypic complementation of KI3 cells requires the synthesis and incorporation of an active form of mSlc35a3 in membranes of the secretory pathway (ER/Golgi apparatus). To exclude incorrect membrane insertion or organelle localization as a cause for the inability of these mutants to transport UDP-GlcNAc, two approaches were undertaken. First, localization of the C-terminally GFP-tagged mutants was evaluated by confocal microscopy. KI3 cells transformed with a plasmid carrying different mutants and CL were grown to an $OD_{600} = 2$, and the cellular localization of the GFP fluorescence signal was analyzed. Similar to CL-GFP– expressing cells, perinuclear fluorescence was observed for all mutants tested, a pattern consistent with expression in the secretory pathway (Fig. 4*A*). Second, membranes were isolated by ultracentrifugation, and proteins abundant in these membrane fractions were separated by SDS-PAGE and analyzed by in-gel fluorescence. As shown in Fig. 4*B*, a predominant band for all mutants with mobility close to the 60-kDa marker was observed. This is consistent with the calculated molecular mass of 55 kDa corresponding to the fusion protein mSlc35a3–GFP (Fig. 4). In agreement with the microscopy data, but not with whole-cell fluorescence results (Fig. S2), the intensity of the main band of mutant 44 was slightly lower compared with the others. Taken together, these

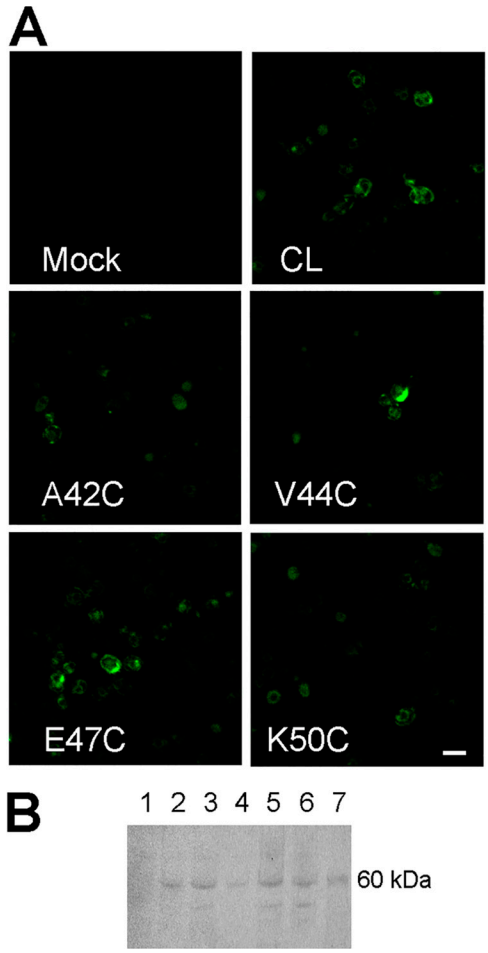

Figure 4. Localization and membrane insertion of inactive mutants. *A,* cells transformed with the empty vector pE4 (*Mock*), pE4-CL-GFP, and pE4 containing the mutated versions A42C, V44C, E47C, and K50C were grown in −Ura media to an OD = 2, and GFP fluorescence was visualized by confocal microscopy. *Scale bar,* 4 μm. *B,* proteins associated with membranes were obtained by ultracentrifugation and separated by SDS-PAGE, and in-gel fluorescence was determined. The lane numbers on the gel correspond to the follows: *lane 1,* mock; *lane 2,* CL; *lane 3,* A42C; *lane 4,* V44C; *lane 5,* E47C; *lane 6,* K50C; and *lane 7,* mass marker.

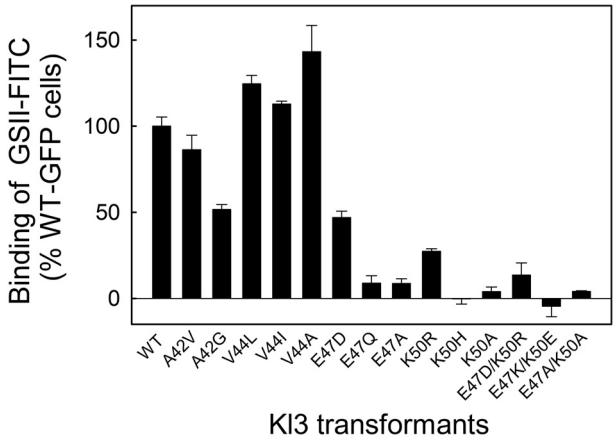

Figure 5. Analysis of single and double mutants of mSlc35a3. Kl3 cells were transformed with the empty vector pE4, pE4-WT–GFP, or pE4 carrying single and double mutants of mSlc35a3 fused to GFP. Cells were grown in −Ura media, isolated, heated for 1 min at 90 °C, and incubated with GSII-FICT for 1 h at room temperature. Fluorescence of the cell suspensions was measured and expressed as a percentage of WT–GFP. *Error bars* represent the mean and S.E. of three independent replicates.

results strongly suggest that all variants were well-integrated into the membranes of the secretory pathway, but in an inactive form.

Analysis of involvement of Glu-47 and Lys-50 residues in mSLC35A3-mediated transport through conservative substitution analysis

To study the importance of residues Ala-42, Val-44, Glu-47, and Lys-50 for the function of mSlc35a3, conservative replacements were made using the WT sequence as backbone. Kl3 cells transformed with the mutant alleles A42V, A42G, V44A, V44I, or V44L fused to GFP showed fluorescence levels similar to those observed for well-expressed proteins (*white bars,* Fig. S3) and values of GSII–FITC binding between 50 and 140% compared with Kl3 cells expressing the WT transporter (Fig. 5). The reduced binding of GSII–FITC in Kl3 cells expressing A42G (50%), but not in A42V (90%), suggests the importance of a lateral group, absent in the small and hydrophilic amino acid glycine. In contrast, cells expressing all Val-44 mutants exhibited an increased abundance of glycoconjugates, suggesting that the changes of V44A, V44I, or V44L improve the function of mSlc35a3 and increase the concentration of luminal UDP-GlcNAc. These results indicate that conservative substitutions of Ala-42 or Val-44 are well-tolerated as revealed by the *in vivo* transport activity. However, our data further suggest that cysteine replacements in these positions are incompatible with the function of mSlc35a3.

To assess the role of glutamic acid 47 for mSLC35A3 activity, mutations to alanine (E47A), aspartic acid (E47D), or glutamine (E47Q) were generated, and Kl3 cells were transformed with the corresponding variants. As shown in Fig. S3, expression of the mutant E47A was not detectable, whereas E47D and E47Q were expressed at similar levels compared with the WT protein. The *in vivo* activity was assessed by incubation of Kl3 transformants with GSII–FITC lectin. Cells expressing the E47D mutant bound 47% of the lectin compared with control cells transformed with the WT protein. By contrast, the substitution E47Q completely abolished the biosynthesis of GlcNAc glycoconjugates and showed no binding. The significance of lysine 50 was examined by substituting Lys-50 with alanine (K50A), histidine (K50H), or arginine (K50R). Kl3 cells were transformed with the corresponding mutant variants, and expression was monitored by whole-cell GFP fluorescence. As is shown in Fig. S3, no expression was detectable for K50H, whereas the K50A and K50R variants were expressed at similar levels to those of the WT protein. Upon incubation of Kl3 cells expressing the K50R mutant with GSII–FITC, low levels of GlcNAc were detected, suggesting severely impaired transport activity.

To explore a possible interaction between both charged amino acids, double mutants were generated and expressed in Kl3 cells (Fig. S3). To elucidate whether a charge misbalance in the individual mutations (E47C or K50C) caused the impairment in transport activity, both charges were neutralized (E47A/K50A). To analyze whether their specific positions in TMH2 are of particular relevance, both residues were interchanged (E47K/K50E). Finally, a mutant containing substitu-

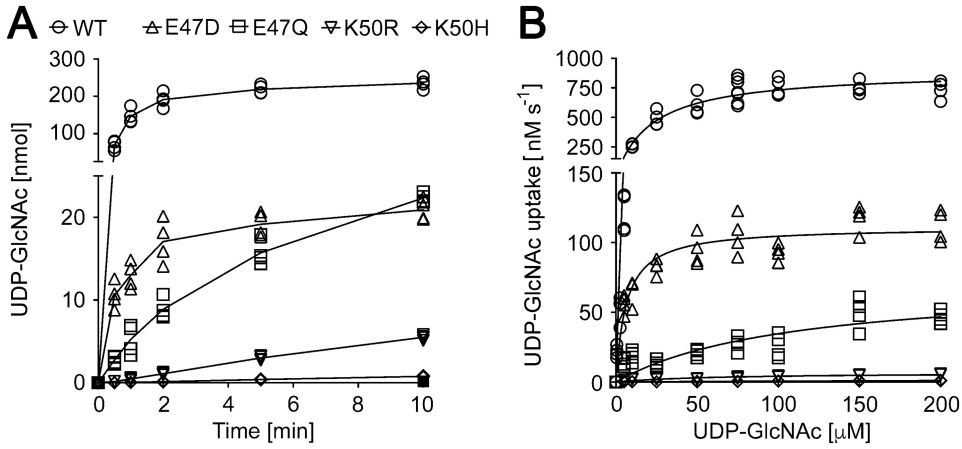

Figure 6. *In vitro* activities of mSlc35a3 and variants. *A,* proteoliposomes containing WT or mutants, preloaded with 30 mM UMP, were incubated with UDP-GlcNAc at a concentration of 50 μM for the indicated time points at 37 °C. UDP-GlcNAc uptakes are expressed in nanomoles normalized to the total protein content in proteoliposomes (four independent replicates). *B,* proteoliposomes containing WT and mutants, preloaded with 30 mM UMP, were incubated with UDP-GlcNAc at varying concentrations (0.5–200 μM) for 30 s at 37 °C. Activity values were normalized to the GFP fluorescence in proteoliposome preparations. For each mSLC35A3 variant, 10 data points (four independent replicates) were acquired, and a hyperbolic function was fitted by nonlinear regression using the Prism 7 application. Best fit kinetic parameters are shown in Table 2 and are represented as the mean ± S.E.

tions of the residues that lead to simultaneous changes in length but conservation of the original charge (E47D/K50R) was generated. As shown in Fig. 5, neutralization of the charge or interchange of the position disrupts the production of GlcNAc glycoconjugates on the surface of Kl3 cells transformed with the corresponding plasmids. Kl3 cells expressing the E47D/K50R mutant bound less than 20% of the lectin compared with cells expressing the WT protein, suggesting an additive effect of the corresponding individual mutations.

Glu-47 and Lys-50 are critical for UDP-GlcNAc/UMP exchange activity of mSlc35a3

Phenotypic complementation of Kl3 cells was used as an efficient way to screen and identify relevant residues. However, limited information could be obtained about the specific properties of the mSlc35a3 variants. To study the UDP-GlcNAc transport properties of mSLC35A3 and the effect of the mutations E47D, E47Q, K50R, and K50H in detail, the WT protein as well as the variants were heterologously expressed in *Saccharomyces cerevisiae*. Membrane proteins were reconstituted into liposomes, and the corresponding proteoliposome preparations, preloaded with UMP, were incubated with UDP-GlcNAc, and nucleotide sugar uptake was evaluated by MS. UDP-GlcNAc uptake was saturable in a time- and concentration-dependent manner (Fig. 6, *A* and *B*). Determinations of the kinetic parameters of UDP-GlcNAc transport activity mediated by the WT mSLC35A3 revealed a K_m of 22 μM and V_{max} of 894 nM s^{-1} (Table 2). In contrast, proteoliposomes containing the corresponding mutant variants E47D, E47Q, K50R, or K50H showed UDP-GlcNAc accumulation over time with variable levels between 1 and 10% compared with the WT (Fig. 6*B*). Velocities were dramatically affected in Glu-47 and Lys-50 substitutions with values close to 10 and 1% of WT mSlc35a3. The apparent affinities of the variants for UDP-GlcNAc showed a decrease for all mutants except for E47D (Table 2).

Table 2
Kinetic parameters of UDP-GlcNAc transport mediated by mSlc35a3 and selected mutants

	WT	E47D	E47Q	K50R	K50H
K_m (μM)	22 ± 3	7 ± 1	108 ± 46	63 ± 17	307 ± 152
V_{max} (nM s^{-1})	894 ± 29	114 ± 4	72 ± 15	7 ± 1	3 ± 1

EXXK motif is specific to subfamily A members and conserved among species

A multiple alignment generated from the putative TMH2 amino acid sequences of mSlc35a3 and other members of the mouse SLC35 family revealed that the E*XX*K motif containing Glu-47 and Lys-50 is present only in subfamily A (Fig. 7), indicating uniqueness of the motif and possibly providing distinct structural/functional properties. In addition, the motif is found in characterized NSTs across a variety of species ranging from unicellular organisms like *Entamoeba histolytica* (50) and yeast (51) to worms (4), plants (52), and mammals (29, 45). This suggests an early occurrence of this subfamily in eukaryotes and an adaptation to transport diverse substrates during evolution.

Interactions between TMH2/TMH7 and TMH2/TMH8 were predicted by coevolution studies of amino acid residues

Evolutionary constraints on the function and structure of proteins are reflected in conserved interactions between pairs or groups of amino acids (53). To evaluate possible interactions involving residues of TMH2 in the context of the whole protein, the mSlc35a3 sequence was analyzed using the algorithm EVfold_membrane. This algorithm extracts coevolution patterns from multiple sequence alignments using an entropy maximization approach (54). The scoring of evolutionarily constrained pairs, many reflecting interactions between residues close in space, suggests that residues from TMH2 interact with residues of TMH7 and TMH8. As shown in the contact map (Fig. S4) from 330 evolutionary couplings, specifically, the five pairs Val-44/Leu-221, Ile-51/Phe-214, Ile-51/Ser-217, Phe-48/Ser-217, and Ile-55/Ile-210 are predicted to interact between TMH2 and TMH7, and the two pairs Ala-53/Ala-253 and Leu-

```
SLC35F5    MALG---IVILLLVDVIWVASSELTSYVFTQYNFIIWKPWRQQCTRGFRGKPAAFFADAE
SLC35F1    -AEDFHAN--TPVFQSF----LNYILLFLVYTTTLAVRQGEENLLAILRR----------
SLC35F2    ----------TPMLQSF----INYCLLFLVYTLMLAFQSGSDNLLEILRR----------
SLC35F3    TFKTFD----APFTLTWFATNWNFLFFPLYYAGHVCKSTEKQSMKQRYRE--------CC
SLC35F4    TYKNFY----CPFFMTWFSTNWNIMFFPVYYSGHLATAQEKQSPIKKFRE--------CS
SLC35B4    ARTHPGCG----------NIVTFAQFLFIAVEGFLFEA-----N----------L
SLC35B3    FSVE---GFKPYG------WYLTLVQFAFYSVFGLIE-L-----Q----------L
SLC35B1    TRGKYGEGPKQETFTFA--LTLVFIQCVINAMFAKILIQ-----F----------F
SLC35B2    MTGSYGATATSPGEHFTDSQFLVLMNRVLALVVAGLYCV-------------------L
SLC35A5    SAN--EEN----KYD-YLPTTVNVCSELMKLILCILVSLCVIKKE-DHQSRH-LR----C
SLC35A4    LALCHVDG----RVP-FRPSSAVLLTELTKLLLCAFSLLVGWQTWP----------
SLC35A1    TRT-TA------EEL-YFSTTAVCITEVIKLLISVGLL-AKETGSLGRFKAS-LS----E
SLC35A2    ART-LP------GDR-FFATTAVVMAEVLKGLTCLLLLFAQKRGNVKHLVLF-LH----E
SLC35A3    SRT-LKEE----GPR-YLSSTAVVVAEFLKIMACIFLVYKDSKCSVRALNRV-LH----D
SLC35D3    LISRY-------QFSF--LTLVQCLTSSTAALSLELLRRL------GL-----IAVPPFG
SLC35D1    VLTNY-------RFPS--SLCVGLGQMVATVAVLWVGKTL------RV-----VKFPDFD
SLC35D2    LLTTY-------GFPS--PIVLGIGQMATTIMILYVFKLN------KI-----IHFPDFD
SLC35E1    ------------A---GLPPLLRAWRVPPAPPVS------GPGPGPHPASGP--------
SLC35E2    ILSLL-------E---GEPSMLGAVQMLSTTLIG-CVKIFVPCCLYQHKTRL--------
SLC35C1    LLDSP-------SLQLDTPIFVTFYQCLVTSLLCKGLSTLATCCP-GMVDFPTL---NLD
SLC35C2    LTKSF-------HFPLFMT-MLHL----AVIFLFSALSRALVQCS-SHKARVVLSWTDYL
SLC35E3    IYVHH-------GFPNMSLTLVHF----VVTWLG------LYICQ-KL----------
```

Figure 7. Multiple sequence alignment of mSLC35 members. The sequences of the predicted members of family SLC35 from mice were aligned using Clustal Omega. Residues corresponding to TMH2 of mSLC35A3 are *underlined*. The conserved residues of the motif E*XX*K are colored in *red* (Glu) and *blue* (Lys).

49/Val-248 are predicted to interact between TMH2 and TMH8. Our results revealed no coevolution pairs between TMH7 and TMH8 suggesting a localization on opposite sides of TMH2. For the highly conserved residues Glu-47 and Lys-50, no interaction with residues of other TMHs were predicted.

Finally, the 3D structure of the protein was computed using EVfold_membrane, based only on the predicted residue contacts and restrictions imposed by topology (54). The resulting model, shown in Fig. S5, contains 10 TMHs with an arrangement resembling the structure of members of the drug/metabolite transporter (DMT) superfamily that have been crystallized so far (44, 55, 56).

Homology model of mSlc35a3

A homology model of mSlc35a3 was generated using the Phyre2 Protein Fold Recognition Server (57). The model was built on the basis of the structure of Vrg4 (PDB code 5OGE), and the quality of the model was tested using the structure-validated web server Molprobity (58). A comparison of the homology model (Fig. 8) with the model obtained using coevolutionary information (Fig. S5) shows that they are highly similar. The resulting models contain 10 TMHs folded in two with a central cavity limited by TMH2–4 and TMH6–9, whereas TMH5 and TMH10 outside this core structure appear as a zipper. Residues Glu-47 and Lys-50 seem to be oriented to the same side of TMH2 facing the central cavity of the protein (Fig. 8*B*).

Discussion

In this work, a combination of bioinformatic and experimental approaches identified two charged residues, Glu-47 and Lys-50, as potentially important for mouse Slc35a3 function. Conservative substitutions of these amino acids resulted in a severe impairment of mSlc35a3 function with a dramatic reduction in UDP-GlcNAc/UMP exchange, thereby highlighting the critical role of Glu-47 and Lys-50. Shortening the length of the side chain in E47D and elimination of the charge in E47Q affected the UDP-GlcNAc transport capacity of mSlc35a3 (Figs. 5 and 6), indicating the requirement of the negative charge and side-chain length, likely involved in interactions during the UDP-GlcNAc/UMP exchange. Even more dramatic effects were caused by substitutions of Lys-50, which almost completely inactivated UDP-GlcNAc transport activity, both *in vivo* and *in vitro* (Figs. 5 and 6).

An analysis of the topology of the protein indicates that residues that maintain close spatial proximity are embedded in the highly hydrophobic center of TMH2. Charge balance, relative position, or intrahelix interactions of Glu-47 and Lys-50 were explored by generating the double mutants E47A/K50A, E47K/K50E, and E47D/K50R. For all double mutants, the phenotypic complementation assay indicated a very low flux of UDP-GlcNAc into the Golgi lumen suggesting that the relative position of the charges in the TMH2 are critical for mSlc35a3 function.

Sequence comparisons of members of the mouse SLC35 family showed that the motif E*XX*K present in TMH2 is specific to members of SLC35 subfamily A (Fig. 7). The identified substrates for Slc35a1, -a2, and -a3 (CMP-SA, UDP-Gal, and UDP-GlcNAc, respectively) are highly diverse in terms of their nucleotide and sugar residues (29–31). Therefore, it is difficult to directly associate these charged amino acids of the consensus motif with an initial ligand recognition on the cytosolic side of the transporter. However, the corresponding nucleotides are pyrimidines and have a common structure that could be recognized. One hypothesis could be that the negatively charged phosphate group of the nucleotide sugar or the nucleoside monophosphate could interact with these charged residues during ligand recognition. The alteration of the kinetic parameters in the mutants (Table 2) is compatible with the coordination of one or both ligands.

Moreover, the participation of the two charged residues of the consensus motif could be related to a secondary event that is common to all members of subfamily A, *e.g.* the helix–helix interactions or conformational changes as part of an alternating access mechanism. The coevolution analysis of mSlc35a3 predicted an interaction between TMH2 and TMH7 via five con-

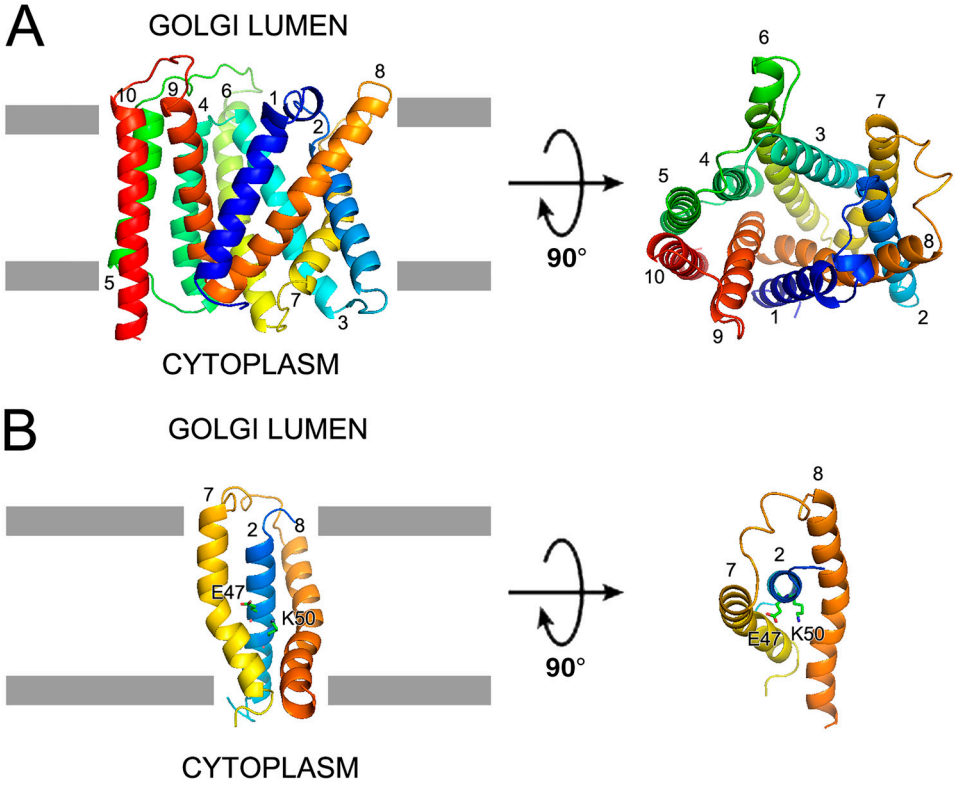

Figure 8. Homology-based model of mSlc35a3. The homology model was generated as was described under "Experimental procedures." *A, ribbon* representation of the structure, viewed from the plane of the membrane (*left*) and luminal side (*right*). *B, ribbon* representation of TMH2, TMH7, and TMH8.

tact points (Fig. S4). Particularly, three of those involved residues Phe-48 (with Ser-217 residue) and Ile-51 (with Phe-214 and Ser-217 residues) that are located right next to Glu-47 and Lys-50 in the sequence of TMH2. Studies on chimeric proteins Slc35a1 and -a2 showed that a swap of the amino acid sequences corresponding to TMH2, TMH3, and TMH7 from Slc35a1 to Slc35a2 conferred CMP-SA specificity in addition to its originally identified substrate UDP-Gal. Moreover, the introduction of Tyr-214 and Ser-216 residues from Slc35a1 at the same position into Slc35a2–TMH7 revealed that they are critically important for the recognition of CMP-SA. Altogether, based on these results it can be assumed that certain residues of TMH7 could be important for the recognition of the substrate, whereas others may be involved in interactions with residues of TMH2 as part of the coupling mechanism.

High-resolution crystal structures have been obtained for three other members of the DMT superfamily, to which the NSTs belong. The structural analyses of SnYddG, a bacterial aromatic amino acid exporter (55), GsGPT, a eukaryotic or 3-phosphoglycerate (3-PGA)/P_i translocator (56), and Vrg4, the GDP-mannose (GDP-Man) transporter from yeast (44), revealed 10 TMHs folded into the N- and a C-terminal halves (55). The structural results for GsGPT, bound to P_i or 3-PGA, showed that the phosphate moieties (P-O_2, O_3, and O_4) of P_i or 3-PGA are recognized by ionic bonds with Lys-204 (TMH4) and Lys-362/Arg-363 (TMH9) and a hydrogen bond with Tyr-339 (TMH8). The glycerate group of 3-PGA specifically interacts via an ionic bond with His-185 (TMH3), a hydrogen bond with Tyr-339 (TMH8), and hydrophobic contacts with Thr-188, Phe-192 (TMH3), and Phe-263 (TMH6). Mutational analyses and molecular dynamics simulations confirmed the significance of these residues. They revealed that Glu-207 (TMH4), the only conserved acidic residue in the positively charged binding pockets, is critical as a molecular switch, interacting with Lys-204 (TMH4) or Arg-363 (TMH9) (59). Sequence comparisons of subfamily members with distinct sugar-phosphate specificities suggest conservation of these residues that interact with the phosphate moieties and variability within the residues that interact with the sugar, hence determining the specificity.

The structure of the yeast GDP-Man transporter Vrg4 was resolved in the apoprotein and GDP-Man–bound forms (44). The results showed that the nucleotide and sugar are accommodated within separate binding pockets. The nucleotide pocket is composed of side chains of the residues Asn-220 and Asn-221 located within TMH7 and Ser-266 (TMH8) that interact with guanine, and Tyr-28 (TMH1), Ser-269 (TMH8) and Tyr-281 (TMH9) that interact with the ribose group. Met-35 (TMH1) interacts with the first phosphate and Lys-289 (TMH9) interacts with the β-phosphate and the glycosidic-bond oxygen. Tyr-114, located within TMH4, is involved in sugar binding via the C2 hydroxyl group on the mannose ring. Based on the structural and mutational analyses, the authors proposed an alternating-access mechanism (44). The interaction of conserved residues from the two inverted repeats TMH1–5 and TMH6–10, Ser-32 (TMH1), Lys-289 (TMH9), Asn-191 (TMH6), and Lys-118 (TMH4), are formed and broken during the transport cycle.

Fig. 8 shows the homology model for mSlc35a3 based on the crystallographic structure of Vrg4. Remarkably, this model is very similar to the coevolution model (Fig. S5). Both models

show 10 TMHs distributed in two halves, TMH1–4 and TMH6–9, defining a central cavity. However, there are significant differences in the distribution of charged residues embedded in the TMHs between Vrg4 and the mSlc35a3 model. The exception is a common Lys on TMH4 (Lys-118 in Vrg4 and Lys-120 in mSlc35a3). A positively charged residue corresponding to the relevant Lys-289 is not present in TMH9 of mSlc35a3 and, on the contrary, no charged residues are present on the TMH2 of Vrg4.

From these data, some common features of the structures of the DMT superfamily (60) begin to emerge. On one side, structural models suggest similar folding for all 10 TMH members despite the low sequence identities between these proteins (about 10%), and an evolutionary adaptation to transport molecules with different chemical characteristics that seem to be based on common folding and mechanism. On the other side, charged residues are involved in the interaction with ligands, particularly with the phosphate groups, and in helix–helix interactions during conformational transitions of the alternating access mechanism. Our results show that mSlc35a3 would have only three charged residues within its transmembrane domains, Glu-47, Lys-50, and Lys-120 (Table 1). The last residue is located in TMH4 and corresponds to Lys-118 from Vrg4, which is proposed to be part of the interaction with the C-half of the inverted repeats during the alternating access mechanism.

The crystal structure of Vrg4 seems to adopt a dimer arrangement, involving both the TMH5 and the TMH10 interface. The localization of the TMH2 on the opposite side of the protein (based on the homology model), seems to rule out an involvement of residues Glu-47 or Lys-50 in the dimerization of mSlc35a3. We speculate that Glu-47 and Lys-50 residues in the context of the interacting helices TMH2–TMH7 and TMH8 are involved in protein–ligand interactions and/or conformational transitions between the N- and the C-terminal halves of the protein, which should be an obligatory step for the exchange UDP-GlcNAc/UMP. However, that leaves open the question of how charged residues located in different TMHs can coordinate ligands to operate a common transport mechanism of NSTs.

Experimental procedures

Materials

Common chemicals used in this work were of analytical grade and were obtained from Sigma. Yeast extract and peptone were obtained from Britannia (Argentina).

Bioinformatic analysis

The primary amino acid sequences of the SLC35 family proteins were analyzed using the following topology predictors: TOPCONS (61), MEMSAT-SVM (62), HMMTOP (63), and TMHMM (64). Sequence alignments were generated using Clustal Omega (65).

Molecular biology

Unless otherwise stated, standard molecular biology protocols were applied as described in Ref. 66. The *Mus musculus slc35a3* gene (mSLC35A3) was PCR-amplified from cDNA (clone ID 5150304, Open Biosystem) using DNA polymerase (Bioline, USA) and primers XhoI–Mmf 5′-GCGGCGCTCGAGATGTCTGCCAACCTAAAATAT-3′ and Mm-EcoRI 5′-CGCCGCGAATTCCTATGCTTTAGTGGGATTTCC-3′. The resulting PCR product was digested with XhoI and EcoRI and subsequently ligated into the pE4 vector (47) to obtain the plasmid pE4-m*slc35a3* for expression in the *K. lactis* mutant 3 (Kl3). To generate a GFP fusion (m*slc35a3*-GFP) in pE4, the m*slc35a3* sequence was introduced into the vector p426Gal-GFP (67) by homologous recombination and subsequently subcloned into the pE4 vector.

In the first step, the PCR product was obtained using the following primers (EcoRI): mouse RECf (5′-TCGACGGATTCTAGAACTAGTGGATCCCCCGAATTCATGTCTGCCAACCTAAAATAT-3′) and mouse RECr (5′-AAATTGACCTTGAAAATATAAATTTTCCCCTGCTTTAGTGGGATTTCCTGC-3′). The plasmid p426Gal-GFP was digested with SmaI and transformed into *S. cerevisiae* FGY217 (kindly provided by Prof. Ljungdahl). The plasmid p426Galm*slc35a3*–GFP, purified from *S. cerevisiae*, was digested with EcoRI to release the insert EcoRI–m*slc35a3*–GFP–EcoRI and subsequently ligated into the vector pE4. The correct orientation was confirmed by colony PCR using appropriate primers. Plasmid p426Gal–GFP was obtained essentially as described previously (67). In brief, the GFP sequence was PCR-amplified from pUG35 plasmid (kindly provided by Dr. Johannes Hegemann), using the following primers: TEVGFPfor (5′-GAAAATTTATATTTTCAAGGTCAATTTTCTAAAGGTGAAGAATTATTCAC-3′) and GFPhisrev (5′-TTAATGATGATGATGATGGTGGTGGTGTTTGTACAATTCATCCATACC-3′). The corresponding PCR fragment was used as template in the second round of PCR using the following primers: RecTEVfor (5′-TCTAGAACTAGTGGATCCCCCCCCGGGGAAAATTTATATTTTCAAGGTC-3′) and Rechisrev (5′-GATAAGCTTGATATCGAATTCCTGCAGTTAATGATGATGATGATGGTGGTGG-3′) to add recombination sequences. Finally, the PCR product was introduced into the pRS426GAL1 plasmid (kindly provided by Dr. James Konopka) digested with SmaI by homologous recombination into the FGY217 yeast strain.

To obtain the CL mutant, the following protocol was used. First, two fragments were obtained by PCR. Fragment A with primers (EcoRI) mouseRECf/C54S/C64Sr and fragment B with primers C184Sf/mouseRECr (Table S2) using m*slc35a3* cDNA as template were used. After purification, both fragments were used in PCR to obtain the full-length fragment with the corresponding serine codons replacing the cysteine codons. The cysteine-unique mutants were generated using the primers listed in Table S2 (L38C to K60C) and employing the megaprimer method (68) in two rounds of PCR. In the first round, a fragment (megaprimer) containing the mutation was obtained in combination with primer (EcoRI)mouseRECf. In the second round, the megaprimer was used in combination with the primer mouseRECr to obtain the full-length version. In both rounds, the CL sequence obtained was used as a template. Finally, single- and double-point mutations of WT-m*slc35a3* were obtained essentially as described for a unique cysteine

mutant using the WT cDNA as template and the corresponding primers (E47Dr, E47Qr, E47Ar, E47Cr, K50Rr, E47K/K50Er, E47D/K50Rr, V44Ar, V44Lr, and V44Ir). The identity of the cloned fragments was confirmed by DNA sequencing.

Yeast strain, transformation, and growth media

For transformation of the *K. lactis mutant 3* (Kl3, Mata, uraA, mnn2-2, arg2$^-$ K$^+$, pKD1$^+$) a lithium acetate/PEG method was utilized (69). Cells were grown in complete YPD media (0.75% yeast extract, 1.13% peptone, 2.2% dextrose), and transformants were selected by their ability to grow at 28 °C in the absence of uracil (−Ura media) on plates containing 0.67% yeast nitrogen base with ammonium sulfate without amino acids (YNB), 0.08% complete supplemented medium minus Ura (Ura$^-$), 2.0% dextrose, and 2.0% agar. WT *K. lactis* cells (Kl8), used as a positive control for the UDP-GlcNAc transporter complementation assays, were grown at 28 °C in YPD media.

Cell surface labeling of K. lactis with GSII–FITC

To assay the activity of the mouse Slc35a3 variants, Kl3 cells transformed with the corresponding pE4 vector (31) were grown overnight in 5 ml of synthetic uracil dropout media to an OD_{600} = 1–2 as described earlier (31). Cells were collected by centrifugation and washed with Solution I (150 mM NaCl, 0.5 mM $CaCl_2$). Cell density was estimated at 600 nm (OD_{600}), and an aliquot, corresponding to 2 units of OD_{600}, was isolated by centrifugation and subsequently resuspended in 200 μl of solution I. GFP fluorescence (excitation, 485 nm/emission, 514 nm) was measured before and after incubation at 90 °C for 1 min to estimate the expression of the corresponding mSLC35A3–GFP variants (WT or mutants). After the 90 °C incubation step, the cells were harvested by centrifugation; the supernatant was discarded; and the pellet was incubated in the presence of 25 μl of GSII–FITC (EY Laboratories) labeling solution (3 parts of lectin + 1 part 150 mM NaCl, 4 mM $CaCl_2$) for 1 h at 25 °C. After this step, the cells were pelleted, washed with 1.5 ml of solution I, and resuspended in 200 μl of solution I before the GFP fluorescence was determined. Fluorescence measurements were normalized to the OD_{600}.

Confocal microscopy of yeast expressing mSlc35a3-GFP

Kl3 cells transformed with pE4 and pE4-MmSLC35A3–GFP (WT or mutants) were mounted on YSB buffer and imaged using an Olympus Fluoview FV1000 spectral laser-scanning confocal microscope with a ×60 oil immersion lens using 473 nm excitation. GFP fluorescence emission was collected between 500 and 550 nm.

Analysis of the membrane integration of the mSlc35a3–GFP fusions using in-gel fluorescence analysis

Total membrane fractions were prepared using glass beads to disrupt the cell pellets derived from 10-ml yeast cultures (OD_{600} = 1–2) in YSB buffer (10% glycerol, 5 mM EDTA, 1 mM phenylmethylsulfonyl fluoride, 50 mM Tris-HCl, pH 7.6). The suspensions were centrifuged at 2,000 × *g* followed by centrifugation of the supernatants at 100,000 × *g* for 1 h. Resulting membrane pellets were resuspended in YSB buffer prior to protein separation by electrophoresis on 12% SDS-polyacrylamide gels (70). Gels were scanned using a Storm 840 molecular imager (Amersham Biosciences) to determine GFP fluorescence.

In vitro transport assay

UDP-*N*-acetyl-α-D-glucosamine (UDP-GlcNAc) was obtained from Sigma. The yeast strain INVScI (Thermo Fisher Scientific) was transformed using the S.c. EasyComp^{TM} transformation kit (Thermo Fisher Scientific). Yeast growth, cell disruption, membrane isolation, membrane protein reconstitution into liposomes, transport activity assays, and MS were performed as described previously in detail (12). Kinetic parameters were calculated by nonlinear regression using the Prism 7 application (GraphPad Software, La Jolla, CA).

Coevolution analysis

The coevolution analysis of residues pairs of MmSlc35a3 was performed using the EV coupling web interface (http://evfold.org/evfold-web/evfold.do)[8] (54).

Homology modeling

The homology model of mSlc35a3 was generated using the Phyre2 Protein Fold Recognition Server (http://www.sbg.bio.ic.ac.uk/phyre2) (57). The model was built on the basis of the structure of Vrg4 (PDB code 5OGE). Model quality was tested using the structure-validate web server Molprobity (http//molprobity.biochem.duke edu)[8] (58).

Author contributions—L. M. B. conceptualization; M. A. T., M. B. F., B. E., C. R., F. L. G. F., and L. M. B. data curation; M. A. T., M. B. F., B. E., C. R., F. L. G. F., and L. M. B. formal analysis; L. M. B. Supervision; B. E. and L. M. B. Funding acquisition; M. A. T., M. B. F., B. E., C. R., F. L. G. F., and L. M. B. investigation; M. A. T., M. B. F., B. E., C. R., F. L. G. F., and L. M. B. methodology; L. M. B. writing-original draft; L. M. B. project administration; M. A. T., M. B. F., B. E., C. R., F. L. G. F., and L. M. B. writing-review and editing.

Acknowledgments—We thank Drs. Javier Santos, Hugo Adamo, and Pablo Schwarzbaum for critical reading of the manuscript and Dr. Gerardo Corradi for technical assistance obtaining the confocal microscopy images.

Addendum—During the review process of this manuscript, new information about the structure of a plant CMP-sialic acid transporter, CSTZM, was made available (Nji, E., Gulati, A., Qureshi, A. A., Coincon, M., and Drew, D. (2019) Structural basis for the delivery of activated sialic acid into Golgi for sialylation. *bioRxiv* CrossRef). This work has shown that residues Glu-42 and Lys-45 on TMH2 are critical for the coordination of the ligand CMP. The coordinates of the structures corresponding to CMP bound CSTZM (PDB code 6I1R) and apo CSTZM (PDB code 6I1Z) have been deposited in the Protein Data Bank.

References

1. Hirschberg, C. B. (2018) My journey in the discovery of nucleotide sugar transporters of the Golgi apparatus. *J. Biol. Chem.* **293,** 12653–12662 CrossRef Medline

[8] Please note that the JBC is not responsible for the long-term archiving and maintenance of this site or any other third party hosted site.

2. Hirschberg, C. B., Robbins, P. W., and Abeijon, C. (1998) Transporters of nucleotide sugars, ATP, and nucleotide sulfate in the endoplasmic reticulum and Golgi apparatus. *Annu. Rev. Biochem.* **67,** 49–69 CrossRef Medline
3. Caffaro, C. E., Koshy, A. A., Liu, L., Zeiner, G. M., Hirschberg, C. B., and Boothroyd, J. C. (2013) A nucleotide sugar transporter involved in glycosylation of the *Toxoplasma* tissue cyst wall is required for efficient persistence of bradyzoites. *PLoS Pathog.* **9,** e1003331 CrossRef Medline
4. Caffaro, C. E., Hirschberg, C. B., and Berninsone, P. M. (2007) Functional redundancy between two *Caenorhabditis elegans* nucleotide sugar transporters with a novel transport mechanism. *J. Biol. Chem.* **282,** 27970–27975 CrossRef Medline
5. Liu, L., and Hirschberg, C. B. (2013) Developmental diseases caused by impaired nucleotide sugar transporters. *Glycoconj. J.* **30,** 5–10 CrossRef Medline
6. Capasso, J. M., and Hirschberg, C. B. (1984) Mechanisms of glycosylation and sulfation in the Golgi apparatus: evidence for nucleotide sugar/nucleoside monophosphate and nucleotide sulfate/nucleoside monophosphate antiports in the Golgi apparatus membrane. *Proc. Natl. Acad. Sci. U.S.A.* **81,** 7051–7055 CrossRef Medline
7. Berninsone, P., Miret, J. J., and Hirschberg, C. B. (1994) The Golgi guanosine diphosphatase is required for transport of GDP-mannose into the lumen of *Saccharomyces cerevisiae* Golgi vesicles. *J. Biol. Chem.* **269,** 207–211 Medline
8. Caffaro, C. E., Hirschberg, C. B., and Berninsone, P. M. (2006) Independent and simultaneous translocation of two substrates by a nucleotide sugar transporter. *Proc. Natl. Acad. Sci. U.S.A.* **103,** 16176–16181 CrossRef Medline
9. Rautengarten, C., Ebert, B., Moreno, I., Temple, H., Herter, T., Link, B., Doñas-Cofré, D., Moreno, A., Saéz-Aguayo, S., Blanco, F., Mortimer, J. C., Schultink, A., Reiter, W. D., Dupree, P., Pauly, M., *et al.* (2014) The Golgi localized bifunctional UDP-rhamnose/UDP-galactose transporter family of *Arabidopsis*. *Proc. Natl. Acad. Sci. U.S.A.* **111,** 11563–11568 CrossRef Medline
10. Bredeston, L. M., Marino-Buslje, C., Mattera, V. S., Buzzi, L. I., Parodi, A. J., and D'Alessio, C. (2017) The conundrum of UDP-Glc entrance into the yeast ER lumen. *Glycobiology* **27,** 64–79 CrossRef Medline
11. Ebert, B., Rautengarten, C., Guo, X., Xiong, G., Stonebloom, S., Smith-Moritz, A. M., Herter, T., Chan, L. J., Adams, P. D., Petzold, C. J., Pauly, M., Willats, W. G., Heazlewood, J. L., and Scheller, H. V. (2015) Identification and characterization of a Golgi-localized UDP-xylose transporter family from *Arabidopsis*. *Plant Cell* **27,** 1218–1227 CrossRef Medline
12. Rautengarten, C., Ebert, B., Liu, L., Stonebloom, S., Smith-Moritz, A. M., Pauly, M., Orellana, A., Scheller, H. V., and Heazlewood, J. L. (2016) The *Arabidopsis* Golgi-localized GDP-L-fucose transporter is required for plant development. *Nat. Commun.* **7,** 12119 CrossRef Medline
13. Saez-Aguayo, S., Rautengarten, C., Temple, H., Sanhueza, D., Ejsmentewicz, T., Sandoval-Ibañez, O., Doñas, D., Parra-Rojas, J. P., Ebert, B., Lehner, A., Mollet, J. C., Dupree, P., Scheller, H. V., Heazlewood, J. L., Reyes, F. C., and Orellana, A. (2017) UUAT1 is a Golgi-localized UDP-uronic acid transporter that modulates the polysaccharide composition of *Arabidopsis* seed mucilage. *Plant Cell* **29,** 129–143 CrossRef Medline
14. Rautengarten, C., Birdseye, D., Pattathil, S., McFarlane, H. E., Saez-Aguayo, S., Orellana, A., Persson, S., Hahn, M. G., Scheller, H. V., Heazlewood, J. L., and Ebert, B. (2017) The elaborate route for UDP-arabinose delivery into the Golgi of plants. *Proc. Natl. Acad. Sci. U.S.A.* **114,** 4261–4266 CrossRef Medline
15. Li, L. X., Rautengarten, C., Heazlewood, J. L., and Doering, T. L. (2018) Xylose donor transport is critical for fungal virulence. *PLoS Pathog.* **14,** e1006765 CrossRef Medline
16. Li, L. X., Rautengarten, C., Heazlewood, J. L., and Doering, T. L. (2018) UDP-glucuronic acid transport is required for virulence of *Cryptococcus neoformans*. *MBio* **9,** e02319-17 Medline
17. Ebert, B., Rautengarten, C., McFarlane, H. E., Rupasinghe, T., Zeng, W., Ford, K., Scheller, H. V., Bacic, A., Roessner, U., Persson, S., and Heazlewood, J. L. (2018) A Golgi UDP-GlcNAc transporter delivers substrates for *N*-linked glycans and sphingolipids. *Nat. Plants* **4,** 792–801 CrossRef Medline
18. Ashikov, A., Routier, F., Fuhlrott, J., Helmus, Y., Wild, M., Gerardy-Schahn, R., and Bakker, H. (2005) The human solute carrier gene SLC35B4 encodes a bifunctional nucleotide sugar transporter with specificity for UDP-xylose and UDP-*N*-acetylglucosamine. *J. Biol. Chem.* **280,** 27230–27235 CrossRef Medline
19. Klein, M. C., Zimmermann, K., Schorr, S., Landini, M., Klemens, P. A. W., Altensell, J., Jung, M., Krause, E., Nguyen, D., Helms, V., Rettig, J., Fecher-Trost, C., Cavalié, A., Hoth, M., Bogeski, I., *et al.* (2018) AXER is an ATP/ADP exchanger in the membrane of the endoplasmic reticulum. *Nat. Commun.* **9,** 3489 CrossRef Medline
20. Martinez-Duncker, I., Dupré, T., Piller, V., Piller, F., Candelier, J. J., Trichet, C., Tchernia, G., Oriol, R., and Mollicone, R. (2005) Genetic complementation reveals a novel human congenital disorder of glycosylation of type II, due to inactivation of the Golgi CMP-sialic acid transporter. *Blood* **105,** 2671–2676 CrossRef Medline
21. Mohamed, M., Ashikov, A., Guillard, M., Robben, J. H., Schmidt, S., van den Heuvel, B., de Brouwer, A. P., Gerardy-Schahn, R., Deen, P. M., Wevers, R. A., Lefeber, D. J., and Morava, E. (2013) Intellectual disability and bleeding diathesis due to deficient CMP–sialic acid transport. *Neurology* **81,** 681–687 CrossRef Medline
22. Ng, B. G., Buckingham, K. J., Raymond, K., Kircher, M., Turner, E. H., He, M., Smith, J. D., Eroshkin, A., Szybowska, M., Losfeld, M. E., Chong, J. X., Kozenko, M., Li, C., Patterson, M. C., Gilbert, R. D., *et al.* (2013) Mosaicism of the UDP-galactose transporter SLC35A2 causes a congenital disorder of glycosylation. *Am. J. Hum. Genet.* **92,** 632–636 CrossRef Medline
23. Kodera, H., Nakamura, K., Osaka, H., Maegaki, Y., Haginoya, K., Mizumoto, S., Kato, M., Okamoto, N., Iai, M., Kondo, Y., Nishiyama, K., Tsurusaki, Y., Nakashima, M., Miyake, N., Hayasaka, K., *et al.* (2013) *De novo* mutations in SLC35A2 encoding a UDP-galactose transporter cause early-onset epileptic encephalopathy. *Hum. Mutat.* **34,** 1708–1714 CrossRef Medline
24. Edvardson, S., Ashikov, A., Jalas, C., Sturiale, L., Shaag, A., Fedick, A., Treff, N. R., Garozzo, D., Gerardy-Schahn, R., and Elpeleg, O. (2013) Mutations in SLC35A3 cause autism spectrum disorder, epilepsy and arthrogryposis. *J. Med. Genet.* **50,** 733–739 CrossRef Medline
25. Lübke, T., Marquardt, T., Etzioni, A., Hartmann, E., von Figura, K., and Körner, C. (2001) Complementation cloning identifies CDG-IIc, a new type of congenital disorders of glycosylation, as a GDP-fucose transporter deficiency. *Nat. Genet.* **28,** 73–76 CrossRef Medline
26. Lühn, K., Wild, M. K., Eckhardt, M., Gerardy-Schahn, R., and Vestweber, D. (2001) The gene defective in leukocyte adhesion deficiency II encodes a putative GDP-fucose transporter. *Nat. Genet.* **28,** 69–72 CrossRef Medline
27. Dauber, A., Ercan, A., Lee, J., James, P., Jacobs, P. P., Ashline, D. J., Wang, S. R., Miller, T., Hirschhorn, J. N., Nigrovic, P. A., and Sackstein, R. (2014) Congenital disorder of fucosylation type 2c (LADII) presenting with short stature and developmental delay with minimal adhesion defect. *Hum. Mol. Genet* **23,** 2880–2887 CrossRef Medline
28. Furuichi, T., Kayserili, H., Hiraoka, S., Nishimura, G., Ohashi, H., Alanay, Y., Lerena, J. C., Aslanger, A. D., Koseki, H., Cohn, D. H., Superti-Furga, A., Unger, S., and Ikegawa, S. (2009) Identification of loss-of-function mutations of SLC35D1 in patients with Schneckenbecken dysplasia, but not with other severe spondylodysplastic dysplasias group diseases. *J. Med. Genet.* **46,** 562–568 CrossRef Medline
29. Eckhardt, M., Mühlenhoff, M., Bethe, A., and Gerardy-Schahn, R. (1996) Expression cloning of the Golgi CMP-sialic acid transporter. *Proc. Natl. Acad. Sci. U.S.A.* **93,** 7572–7576 CrossRef Medline
30. Miura, N., Ishida, N., Hoshino, M., Yamauchi, M., Hara, T., Ayusawa, D., and Kawakita, M. (1996) Human UDP-galactose translocator: molecular cloning of a complementary DNA that complements the genetic defect of a mutant cell line deficient in UDP-galactose translocator. *J. Biochem.* **120,** 236–241 CrossRef Medline
31. Guillen, E., Abeijon, C., and Hirschberg, C. B. (1998) Mammalian Golgi apparatus UDP-*N*-acetylglucosamine transporter: molecular cloning by phenotypic correction of a yeast mutant. *Proc. Natl. Acad. Sci. U.S.A.* **95,** 7888–7892 CrossRef Medline

32. Eckhardt, M., Gotza, B., and Gerardy-Schahn, R. (1999) Membrane topology of the mammalian CMP-sialic acid transporter. *J. Biol. Chem.* **274,** 8779–8787 CrossRef Medline
33. Aoki, K., Ishida, N., and Kawakita, M. (2003) Substrate recognition by nucleotide sugar transporters: further characterization of substrate recognition regions by analyses of UDP-galactose/CMP-sialic acid transporter chimeras and biochemical analysis of the substrate specificity of parental and chimeric transporters. *J. Biol. Chem.* **278,** 22887–22893 CrossRef Medline
34. Aoki, K., Ishida, N., and Kawakita, M. (2001) Substrate recognition by UDP-galactose and CMP-sialic acid transporters. Different sets of transmembrane helices are utilized for the specific recognition of UDP-galactose and CMP-sialic acid. *J. Biol. Chem.* **276,** 21555–21561 CrossRef Medline
35. Takeshima-Futagami, T., Sakaguchi, M., Uehara, E., Aoki, K., Ishida, N., Sanai, Y., Sugahara, Y., and Kawakita, M. (2012) Amino acid residues important for CMP-sialic acid recognition by the CMP-sialic acid transporter: analysis of the substrate specificity of UDP-galactose/CMP-sialic acid transporter chimeras. *Glycobiology* **22,** 1731–1740 CrossRef Medline
36. Maggioni, A., von Itzstein, M., Rodríguez Guzman, I. B., Ashikov, A., Stephens, A. S., Haselhorst, T., and Tiralongo, J. (2013) Characterisation of CMP-sialic acid transporter substrate recognition. *Chembiochem* **14,** 1936–1942 CrossRef Medline
37. Thomsen, B., Horn, P., Panitz, F., Bendixen, E., Petersen, A. H., Holm, L. E., Nielsen, V. H., Agerholm, J. S., Arnbjerg, J., and Bendixen, C. (2006) A missense mutation in the bovine SLC35A3 gene, encoding a UDP-*N*-acetylglucosamine transporter, causes complex vertebral malformation. *Genome Res.* **16,** 97–105 CrossRef Medline
38. Marini, C., Hardies, K., Pisano, T., May, P., Weckhuysen, S., Cellini, E., Suls, A., Mei, D., Balling, R., Jonghe, P. D., Helbig, I., Garozzo, D., EuroEPINOMICS consortium AR working group, and Guerrini, R. (2017) Recessive mutations in SLC35A3 cause early onset epileptic encephalopathy with skeletal defects. *Am. J. Med. Genet. A* **173,** 1119–1123 CrossRef Medline
39. Edmondson, A. C., Bedoukian, E. C., Deardorff, M. A., McDonald-McGinn, D. M., Li, X., He, M., and Zackai, E. H. (2017) A human case of SLC35A3-related skeletal dysplasia. *Am. J. Med. Genet. A* **173,** 2758–2762 CrossRef Medline
40. Bruneel, A., Cholet, S., Drouin-Garraud, V., Jacquemont, M. L., Cano, A., Mégarbané, A., Ruel, C., Cheillan, D., Dupré, T., Vuillaumier-Barrot, S., Seta, N., and Fenaille, F. (2018) Complementarity of electrophoretic, mass spectrometric, and gene sequencing techniques for the diagnosis and characterization of congenital disorders of glycosylation. *Electrophoresis* **39,** 3123–3132 CrossRef Medline
41. Maszczak-Seneczko, D., Sosicka, P., Olczak, T., Jakimowicz, P., Majkowski, M., and Olczak, M. (2013) UDP-*N*-acetylglucosamine transporter (SLC35A3) regulates biosynthesis of highly branched *N*-glycans and keratan sulfate. *J. Biol. Chem.* **288,** 21850–21860 CrossRef Medline
42. Maszczak-Seneczko, D., Sosicka, P., Kaczmarek, B., Majkowski, M., Luzarowski, M., Olczak, T., and Olczak, M. (2015) UDP-galactose (SLC35A2) and UDP-*N*-acetylglucosamine (SLC35A3) transporters form glycosylation-related complexes with mannoside acetylglucosaminyltransferases (Mgats). *J. Biol. Chem.* **290,** 15475–15486 CrossRef Medline
43. Carey, D. J., Sommers, L. W., and Hirschberg, C. B. (1980) CMP-*N*-acetylneuraminic acid: isolation from and penetration into mouse liver microsomes. *Cell* **19,** 597–605 CrossRef Medline
44. Parker, J. L., and Newstead, S. (2017) Structural basis of nucleotide sugar transport across the Golgi membrane. *Nature* **551,** 521–524 CrossRef Medline
45. Ishida, N., Yoshioka, S., Chiba, Y., Takeuchi, M., and Kawakita, M. (1999) Molecular cloning and functional expression of the human Golgi UDP-*N*-acetylglucosamine transporter. *J. Biochem.* **126,** 68–77 CrossRef Medline
46. Andersen, P. K., Veng, L., Juul-Madsen, H. R., Vingborg, R. K., Bendixen, C., and Thomsen, B. (2007) Gene expression profiling, chromosome assignment and mutational analysis of the porcine Golgi-resident UDP-*N*-acetylglucosamine transporter SLC35A3. *Mol. Membr. Biol.* **24,** 519–530 CrossRef Medline
47. Abeijon, C., Robbins, P. W., and Hirschberg, C. B. (1996) Molecular cloning of the Golgi apparatus uridine diphosphate-*N*-acetylglucosamine transporter from *Kluyveromyces lactis*. *Proc. Natl. Acad. Sci. U.S.A.* **93,** 5963–5968 CrossRef Medline
48. Heijne, G. (1986) The distribution of positively charged residues in bacterial inner membrane proteins correlates with the trans-membrane topology. *EMBO J.* **5,** 3021–3027 CrossRef Medline
49. Illergård, K., Kauko, A., and Elofsson, A. (2011) Why are polar residues within the membrane core evolutionary conserved? *Proteins* **79,** 79–91 CrossRef Medline
50. Bredeston, L. M., Caffaro, C. E., Samuelson, J., and Hirschberg, C. B. (2005) Golgi and endoplasmic reticulum functions take place in different subcellular compartments of *Entamoeba histolytica*. *J. Biol. Chem.* **280,** 32168–32176 CrossRef Medline
51. Tabuchi, M., Tanaka, N., Iwahara, S., and Takegawa, K. (1997) The *Schizosaccharomyces pombe* gms1+ gene encodes an UDP-galactose transporter homologue required for protein galactosylation. *Biochem. Biophys. Res. Commun.* **232,** 121–125 CrossRef Medline
52. Temple, H., Saez-Aguayo, S., Reyes, F. C., and Orellana, A. (2016) The inside and outside: topological issues in plant cell wall biosynthesis and the roles of nucleotide sugar transporters. *Glycobiology* **26,** 913–925 CrossRef Medline
53. Marks, D. S., Hopf, T. A., and Sander, C. (2012) Protein structure prediction from sequence variation. *Nat. Biotechnol.* **30,** 1072–1080 CrossRef Medline
54. Hopf, T. A., Colwell, L. J., Sheridan, R., Rost, B., Sander, C., and Marks, D. S. (2012) Three-dimensional structures of membrane proteins from genomic sequencing. *Cell* **149,** 1607–1621 CrossRef Medline
55. Tsuchiya, H., Doki, S., Takemoto, M., Ikuta, T., Higuchi, T., Fukui, K., Usuda, Y., Tabuchi, E., Nagatoishi, S., Tsumoto, K., Nishizawa, T., Ito, K., Dohmae, N., Ishitani, R., and Nureki, O. (2016) Structural basis for amino acid export by DMT superfamily transporter YddG. *Nature* **534,** 417–420 CrossRef Medline
56. Lee, Y., Nishizawa, T., Takemoto, M., Kumazaki, K., Yamashita, K., Hirata, K., Minoda, A., Nagatoishi, S., Tsumoto, K., Ishitani, R., and Nureki, O. (2017) Structure of the triose-phosphate/phosphate translocator reveals the basis of substrate specificity. *Nat. Plants* **3,** 825–832 CrossRef Medline
57. Kelley, L. A., Mezulis, S., Yates, C. M., Wass, M. N., and Sternberg, M. J. (2015) The Phyre2 web portal for protein modeling, prediction and analysis. *Nat. Protoc.* **10,** 845–858 CrossRef Medline
58. Chen, V. B., Arendall, W. B., III, Headd J. J., Keedy, D. A., Immormino, R. M., Kapral, G. J., Murray, L. W., Richardson, J. S., and Richardson, D. C. (2010) MolProbity: all-atom structure validation for macromolecular crystallography. *Acta Crystallogr. D* Biol. Crystallogr. **66,** 12–21 CrossRef Medline
59. Takemoto, M., Lee, Y., Ishitani, R., and Nureki, O. (2018) Free energy landscape for the entire transport cycle of triose-phosphate/phosphate translocator. *Structure* **26,** 1284–1296.e4 CrossRef Medline
60. Jack, D. L., Yang, N. M., and Saier, M. H., Jr. (2001) The drug/metabolite transporter superfamily. *Eur. J. Biochem.* **268,** 3620–3639 CrossRef Medline
61. Tsirigos, K. D., Peters, C., Shu, N., Käll, L., and Elofsson, A. (2015) The TOPCONS web server for consensus prediction of membrane protein topology and signal peptides. *Nucleic Acids Res.* **43,** W401–W407 CrossRef Medline
62. Nugent, T., and Jones, D. T. (2009) Transmembrane protein topology prediction using support vector machines. *BMC Bioinformatics* **10,** 159 CrossRef Medline
63. Tusnády, G. E., and Simon, I. (2001) The HMMTOP transmembrane topology prediction server. *Bioinformatics* **17,** 849–850 CrossRef Medline
64. Krogh, A., Larsson, B., von Heijne, G., and Sonnhammer, E. L. (2001) Predicting transmembrane protein topology with a hidden Markov model: application to complete genomes. *J. Mol. Biol.* **305,** 567–580 CrossRef Medline
65. Sievers, F., and Higgins, D. G. (2018) Clustal Omega for making accurate alignments of many protein sequences. *Protein Sci.* **27,** 135–145 CrossRef Medline

66. Sambrook, J., Fritsch, E. F., and Maniatis, T. (1989) *Molecular Cloning: A Laboratory Manual*, Cold Spring Harbor Laboratory Press, Cold Spring Harbor, NY
67. Newstead, S., Kim, H., von Heijne, G., Iwata, S., and Drew, D. (2007) High-throughput fluorescent-based optimization of eukaryotic membrane protein overexpression and purification in *Saccharomyces cerevisiae*. *Proc. Natl. Acad. Sci. U.S.A.* **104,** 13936–13941 CrossRef Medline
68. Sarkar, G., and Sommer, S. S. (1990) The "megaprimer" method of site-directed mutagenesis. *BioTechniques* **8,** 404–407 Medline
69. Elble, R. (1992) A simple and efficient procedure for transformation of yeasts. *BioTechniques* **13,** 18–20 Medline
70. Laemmli, U. K. (1970) Cleavage of structural proteins during the assembly of the head of bacteriophage T4. *Nature* **227,** 680–685 CrossRef Medline

Conserved Glu-47 and Lys-50 residues are critical for UDP-*N*-acetylglucosamine/UMP antiport activity of the mouse Golgi-associated transporter Slc35a3

M. Agustina Toscanini, M. Belén Favarolo, F. Luis Gonzalez Flecha, Berit Ebert, Carsten Rautengarten and Luis M. Bredeston

J. Biol. Chem. 2019, 294:10042-10054.
doi: 10.1074/jbc.RA119.008827 originally published online May 22, 2019